Deriving surface-energy anisotropy for phenomenological phase-field models of solidification

Sami Majaniemi*
Department of Materials Science and Engineering, McMaster University, 1280 Main Street West, Hamilton, Ontario L8S-4L7; Department of Physics, McGill University, 3600 University Street, Montréal, QC, Canada H3A 2T8

Nikolas Provatas†
Department of Materials Science and Engineering, McMaster University, 1280 Main Street West, Hamilton, Ontario L8S-4L7
(Received 29 June 2008; published 26 January 2009)

The free energy of classical density functional theory of an inhomogeneous fluid at coexistence with its solid is used to describe solidification in two-dimensional hexagonal crystals. A coarse-graining formalism from the microscopic density functional level to the macroscopic single order parameter level is provided. An analytic expression for the surface energy and the angular dependence of its anisotropy is derived and its coefficients related to the two-point direct correlation function of the liquid phase at coexistence.

DOI: 10.1103/PhysRevE.79.011607 PACS number(s): 68.08.−p, 68.35.Md, 64.70.D−, 61.50.Ah

I. INTRODUCTION

Phase-field modeling has seen an explosive growth in recent years, particularly in the study of solidification and solid state transformations. The basic physics of some otherwise complex free boundary problems have been studied using this methodology. Most phase-field models employ a similar approach: one or more phenomenological order parameter equations are coupled to one or more diffusion fields. Dynamical evolution of these fields is simulated by dissipative minimization of a phenomenological free energy, the latter of which is written such as to respect certain symmetries and properties of the physics at hand.

The recent development of second-order matched asymptotic analysis [1] to phase-field models has also made it possible to *quantitatively* simulate free boundary problems of certain solidification phenomena in the limit of quite diffuse interfaces (so-called "thin-interface limit") [2–7]. This has been a significant step toward making phase-field modeling practical in materials science and engineering applications [2,5,6,8–13].

A limitation of traditional phase-field models is that they are formulated in terms of fields that are spatially uniform in a single phase region in equilibrium. This precludes phenomena that arise from the periodic symmetries inherent in crystalline phases, including elastic and plastic deformation, anisotropy and multiple grain orientations. A way around this problem has been to couple the traditional order parameter fields with one or more auxiliary fields describing such features as the density of dislocations, continuum stress and strain fields and the crystal grain orientation. These approaches have proven quite useful in various applications such as polycrystalline solidification. Nevertheless, it has proven quite challenging to incorporate elasto-plasticity, diffusive phase transformation kinetics and anisotropic surface energy effects into a single, consistent formalism.

A recent innovation in phase-field modeling has seen the introduction of the so-called phase-field crystal (PFC) methodology [14–18]. This formalism has made it possible to incorporate the kinetics of phase transformations with properties of solids that arise due to their periodic structure. This includes elastic strains, topological defects, vacancy diffusion and polycrystalline grain boundary interactions. PFC models have been applied to several phenomena [19]. These include grain growth and epitaxial growth [14,15,20], dislocation flow and rapid strain relaxation in crystals [16,17], and spinodal decomposition in binary alloys [18].

An appealing feature of the phase-field crystal methodology is its connection with classical density functional theory (DFT) [18,21–24]. This makes it possible to develop different classes of PFC models whose form and parameters are microscopically motivated. Moreover, the recent use of renormalization group techniques to project the dynamics of the original PFC model onto a set of complex amplitude equations [25] has demonstrated the potential of coarse-graining PFC-type models (or, equivalently, DFT-type models) to large spatial scales. One obvious numerical advantage of this approach is the use of adaptive mesh refinement to numerically simulate experimentally relevant length scales [26].

Another advantage of coarse-graining density functional theories involves the potential of calculating certain parameters that enter phase field models of solidification—or their associated free boundary problems—from microscopic properties. Two critically important parameters for solidification modeling is the surface energy and the angular form of its anisotropy. These are difficult to measure experimentally and are often only estimated in many studies. Analogously, the diffusion constant and atomic attachment mobility are also very difficult to measure. They can be related to properties of transport coefficients theoretically [23,27,28], although these relations rely on parameters that are difficult to measure experimentally.

A step in the direction of using coarse-grained DFTs to calculate microscopic parameters was recently taken by Wu *et al.* [22,29]. They extended an approach of Shih [30] that used a density wave expansion in a free energy functional of an inhomogeneous liquid to tune the parameters of a Ginzburg-Landau (GL) model of freezing. The GL amplitudes were solved for along specific lattice directions and

*majaniem@physics.mcgill.ca
†provata@mcmaster.ca

then substituted back into the GL free energy to compute the corresponding surface energies. Surface energies and their differences were then compared to those predicted by molecular dynamics simulations, obtaining good agreement for fcc iron.

In this paper, a density functional theory of an inhomogeneous liquid is directly coarse grained in two spatial dimensions using a single mode density wave expansion of the density. A simple projection operator method [31,32] is applied to the amplitude equations obtained from the density expansion to yield an analytic and a numerical approximation of the surface energy and its anisotropy. This paper is organized as follows. Section II presents the density functional theory used in this work. Section III uses volume averaging to coarse grain the free energy functional, leading to a GL-type model written in terms of three amplitudes. Section IV presents a formalism for semi-analytically calculating the anisotropic surface energy from this Ginzburg-Landau model. Section V compares the results of our semianalytical derivation to numerical simulations from the full nonlinear Ginzburg-Landau model. Section VI proposes a simple procedure for going from a three amplitude representation of the of the original DFT to a an effective single order parameter free energy.

II. CLASSICAL DENSITY FUNCTIONAL THEORY

A. Free energy functional

The classical density functional used in this work is written as

$$F_1[\rho] \equiv F_A[\rho] + F_B[\rho] + F_C[\rho], \tag{1}$$

where each term is defined in terms of the dimensionless field $\rho \equiv n_0/\bar{\rho}_0$, where n_0 is the atomic number density and $\bar{\rho}_0$ is the average liquid number density at solid-liquid coexistence. In these units, F_1 represents the dimensional free energy divided by $k_B T\bar{\rho}$, where k_B is Boltzmann's constant and T is temperature. The units of F_1 are thus a volume.

The terms of F_1 are as follows:

$$F_A \equiv \int d\mathbf{r} \int d\mathbf{r}'\, \delta\rho(\mathbf{r})\delta(\mathbf{r}-\mathbf{r}')\delta\rho(\mathbf{r}'), \tag{2}$$

where $\delta\rho \equiv \rho - 1$. This term represents the local short-range interaction part of the free energy. Nonlocal long-range interactions are contained in F_B,

$$F_B \equiv -\int d\mathbf{r} \int d\mathbf{r}'\, \delta\rho(\mathbf{r})c(\mathbf{r}-\mathbf{r}')\delta\rho(\mathbf{r}'), \tag{3}$$

where $c(\mathbf{r}-\mathbf{r}') \equiv \bar{\rho}_0 c^{\exp}(\mathbf{r}-\mathbf{r}')$, with $c^{\exp}(\mathbf{r}-\mathbf{r}')$ being the experimental two-point direct correlation function of the fluid phase at solid-liquid coexistence. The third term in Eq. (1) represents the ideal gas (noninteracting) contribution to the total free energy

$$F_C \equiv \int d\mathbf{r}\{\rho(\mathbf{r})\ln\rho(\mathbf{r}) - \delta\rho(\mathbf{r})\}. \tag{4}$$

B. Density wave expansion of $\rho(\mathbf{r})$

In what follows, we will expand the free energy using a one-mode approximation given by

$$\rho(\mathbf{r}) \equiv \frac{n_0}{\bar{\rho}_0} = 1 + \sum_{n=1}^{3} A_n(\mathbf{r})e^{\imath\mathbf{K}^n\cdot\mathbf{r}} + \text{c.c.}, \tag{5}$$

where $A_n(\mathbf{r})$ are dimensionless spatially dependent amplitudes and the symbol c.c. denotes complex conjugate. For the two-dimensional (2D) hexagonal crystal structure considered here, the reciprocal lattice vectors $\mathbf{K}^n$ are [in units of the inverse lattice spacing $q_0 = 4\pi/(\sqrt{3}a)$, where a is the lattice constant]

$$\mathbf{K}^1 \equiv \mathbf{j}, \quad \mathbf{K}^2 \equiv -\frac{\sqrt{3}}{2}\mathbf{i} - \frac{1}{2}\mathbf{j}, \quad \mathbf{K}^3 \equiv +\frac{\sqrt{3}}{2}\mathbf{i} - \frac{1}{2}\mathbf{j}. \tag{6}$$

In general the amplitudes can be decomposed as

$$A_n(\mathbf{r}) \equiv a_n(\mathbf{r})e^{\imath\Theta_n(\mathbf{r})}, \tag{7}$$

where $a^n(\mathbf{r})$ is a real amplitude corresponding to the density wave n, while $\imath\Theta_n(\mathbf{r})$ is a phase factor required for taking into account the effects of long-range elasticity and small scale defect structure.

III. DERIVATION OF AMPLITUDE MODELS

A. Complex amplitude equations

This section uses a volume averaging technique to coarse grain F_A, F_B, and F_C into functionals of the slowly varying order parameter fields $A_n(\mathbf{r})$, which are analogous to those used in traditional phase-field or Ginzurg-Landau theories. The volume averaging method is described in Appendix A. Loosely speaking coarse graining can be thought of as a procedure by which the terms of the free energy are homogenized over lengths scales that are large compared to the lattice constant but still small compared to the detail of most microstructures.

The first step is to substitute the density expansion (5) into the terms of the free energy F_A, F_B, and F_C. The nonlocal term F_B will generate four terms of the form

$$I_1 \equiv \sum_{n,m=1}^{3} \int d\mathbf{r}' \int d\mathbf{r} A_n(\mathbf{r})\zeta_n^{\pm}(\mathbf{r})c(\mathbf{r}-\mathbf{r}')A_m(\mathbf{r}')\zeta_m^{\pm}(\mathbf{r}'), \tag{8}$$

where $\zeta_n^{\pm}(\mathbf{r}) \equiv e^{\pm i\mathbf{K}^n\cdot\mathbf{r}}$. To coarse grain terms of the form I_1, we expand the slowly varying amplitudes $A_n(\mathbf{r}')$ to second order about $\mathbf{r}' = \mathbf{r}$ according to

$$\begin{aligned} A_n(\mathbf{r}') &\equiv a_n(\mathbf{r}')e^{\imath\Theta_n(\mathbf{r}')} \\ &= A_n(\mathbf{r}) + (r_i' - r_i)\partial_i A_n(\mathbf{r}) \\ &\quad + \frac{1}{2}(r_i' - r_i)(r_j' - r_j)\partial_i\partial_j A_n(\mathbf{r}) + \cdots, \end{aligned} \tag{9}$$

where summation over repeated indices is implied. We also substitute into I_1 the Fourier transform of the two-point correlation function

$$c(|\mathbf{r}-\mathbf{r}'|) \equiv \bar{\rho}_0 c^{\exp}(|\mathbf{r}-\mathbf{r}'|) = \int d\mathbf{k}\hat{c}(|\mathbf{k}|)e^{i\mathbf{k}\cdot(\mathbf{r}'-\mathbf{r})}. \quad (10)$$

The amplitudes $A_n(\mathbf{r}')$ are slowly varying over the domain $\mathbf{r}' < |\mathbf{r}+\vec{L}|$, where $|\vec{L}|$ defines a range of rapid variation of the phase factors $e^{i\Delta\mathbf{K}^n\cdot\mathbf{r}}$, where $\Delta\mathbf{K}^n$ are sums or differences of the $\mathbf{K}^n$ in Eq. (6), emerging from the multiplication of phase factors in Eq. (8). As discussed in Appendix A, terms in I_1 for which $\Delta\mathbf{K}^n \equiv \mathbf{K}_n^n - \mathbf{K}_n^m \neq 0$ vanish under coarse graining, while those for which $\Delta\mathbf{K}^n = 0$ have nonzero volume averages. In other words, the amplitude equations will hold for scales $kq_0 \gg 1$, where q_0 is the inverse lattice constant.

The density expansion (5) is also used to transform the terms F_A and F_C into functionals of $A_n(\mathbf{r})$. For simplicity, the reference free energy F_C was only expanded to fourth order in the $\delta\rho(\mathbf{r})$. The resulting expressions for F_A and F_C do not contain derivatives $A(\mathbf{r})$. The resonance conditions described at the end of the previous paragraph can again be used to determine which terms of the potential part of the free energy survive coarse graining.

The results of coarse graining on $F_A[\rho]$, $F_B[\rho]$, and $F_C[\rho]$ yield, after some straightforward but lengthly algebra, the following free energy functional in terms of the $A_n(\mathbf{r})$:

$$F = \int d\mathbf{r} \sum_{n=1}^{3} A_n(\mathbf{r})(-M_2)(\mathbf{K}^n\cdot\nabla)^2 A_n(\mathbf{r}) + \int d\mathbf{r} V(\mathbf{r}), \quad (11)$$

where $\nabla \equiv \mathbf{i}\partial_x + \mathbf{j}\partial_y$, and the potential V is defined as

$$V(\mathbf{r}) \equiv \sum_n [3 - 2\hat{c}(|\mathbf{K}^n|)]a_n^2 - \cos\left(\sum_n \Theta_n(\mathbf{r})\right) a_1 a_2 a_3 + 6[(a_1a_2)^2 + (a_1a_3)^2 + (a_2a_3)^2] + \frac{3}{2}\sum_n a_n^4. \quad (12)$$

The function M_2 is defined by

$$M_2(|\mathbf{K}^n|) \equiv \frac{\hat{c}^{(2)}(|\mathbf{K}^n|)}{|\mathbf{K}^n|^2} - \frac{\hat{c}^{(1)}(|\mathbf{K}^n|)}{|\mathbf{K}^n|^3}, \quad (13)$$

where hereafter $|\mathbf{K}^n| \equiv q_0$ and the superscripts (2) and (1) denote second and first derivatives, respectively. In the special case where the correlation function is chosen to reproduce the original PFC model [18], the free energy in Eq. (11) is, to the lowest order in derivatives, equivalent to the Lyapunov functional constructed from the equations of motion of Ref. [25]. It should be noted that in Ref. [25] the operator $(\mathbf{K}^n\cdot\nabla)^2$ is replaced by ∇^2 terms since there the amplitude equations are derived directly from the PFC model, which includes a ∇^2 operator for the conservation of chemical potential.

B. Real amplitude equations

To obtain the isotropic and anisotropic contributions of the surface energy of a crystal interface, we leave out, in the first approximation, the phase factors from the complex amplitudes by setting $\Theta_n = 0$. Thus, $A_n = a_n$ in the free energy Eq. (11) and $\cos\{\Sigma_n[\Theta_n(r)]\} = 1$ in the potential $V(\mathbf{r})$. The variation of the resulting F with respect to the real a_n then yields the following Euler-Lagrange equation for a_1:

$$m_1\partial_u^2 a_1 = 2[3 - 2\hat{c}(q_0)]a_1 - a_2a_3 + 6a_1^3 + 12a_1(a_2^2 + a_3^2), \quad (14)$$

where the equation has been written in a curvilinear coordinate frame local to the interface, with coordinate transverse to the interface denoted by u. Two more equations for a_2 and a_3 that are obtained by permutation of the symbols in Eq. (14). We have defined in Eq. (14)

$$m_n \equiv -2M_2(|\mathbf{K}^n|)(\mathbf{n}\cdot\mathbf{K}^n)^2, \quad (15)$$

where $\mathbf{n} = \cos\theta\mathbf{i} + \sin\theta\mathbf{j}$ is the surface normal whose direction forms an angle θ with a (reference) x axis. Since M_2 is negative, the "mass" m_n is a positive number.

IV. DERIVING SURFACE ENERGY OF THE THREE-AMPLITUDE MODEL

A. Expression for surface energy

The surface energy per unit length (L_y) of the multiorder parameter theory can be calculated by writing

$$\frac{F}{L_y} = \int du\left\{\frac{1}{2}\dot{\mathbf{x}}^T M\dot{\mathbf{x}} + V(\mathbf{x})\right\}, \quad (16)$$

where the shorthand notation $\dot{\mathbf{x}} \equiv \partial_u\mathbf{x}$, $\mathbf{x} = (a_1, a_2, a_3)^T$ has been used here, and M is the mass matrix, $M = \mathrm{diag}(m_1, m_2, m_3)$. Specifically, the Euler-Lagrange equations from Eq. (16) read

$$-M\ddot{\mathbf{x}} + \nabla_{\mathbf{x}}V(\mathbf{x}) = 0, \quad (17)$$

which make $\frac{1}{2}\dot{\mathbf{x}}^T M\dot{\mathbf{x}} = V(\mathbf{x}) + h$, where the constant h is zero for properly chosen boundary conditions. In Eq. (17) we have also introduced $\nabla_{\mathbf{x}} \equiv \mathbf{e}_{x_1}\partial_{x_1} + \cdots + \mathbf{e}_{x_3}\partial_{x_3}$, where $\mathbf{e}_{x_1} \equiv (1,0,0)$, $\mathbf{e}_{x_2} \equiv (0,1,0)$, $\mathbf{e}_{x_3} \equiv (0,0,1)$. Writing Eq. (16) in terms of the optimized solutions of Eq. (17), denoted $\mathbf{x}^*$, gives

$$\frac{F}{L_y} \equiv \sigma_3 = \int du(\dot{\mathbf{x}}^*)^T M\dot{\mathbf{x}}^* \quad (18)$$

for the total surface energy σ_3 (the subscript 3 refers to the number of amplitudes a_n that we will be using below for the hexagonal lattices). Note that the potential V is implicit in Eq. (18) through $\mathbf{x}^*$.

For the model studied here, it will be shown to good numerical accuracy that the total surface tension will take the following form:

$$\sigma_3 = \sigma^{\mathrm{iso}}[1 + \epsilon\cos(6\theta) + \cdots], \quad (19)$$

where θ is the angle θ that the surface normal makes with the reference direction, σ^{iso} is the isotropic part of the surface tension, and ϵ is the anisotropy factor. Equation (19) is also derived analytically for a simple case in Appendix B.

B. Scaling form of the amplitude fields

To solve for the surface tension semianalytically from Eqs. (14), it is assumed that these equations have solutions of the form

$$a_1 = f_1(u/\xi_1, m_1, m_2, m_3), \tag{20}$$

$$a_2 = f_2(u/\xi_2, m_1, m_2, m_3), \tag{21}$$

$$a_3 = f_3(u/\xi_3, m_1, m_2, m_3), \tag{22}$$

where ξ_i are correlation lengths corresponding to each amplitude and u is the coordinate transverse to the interface.

To avoid messy algebra but still make progress toward the goal of approximating the surface energy and its anisotropic form, the scaling forms in Eqs. (20)–(22) will be further assumed to simplify to the form

$$a_n \approx f_n(u/\xi_n) \approx f(u/\xi_n). \tag{23}$$

This assumption will allow us to obtain analytically a crude but illuminating approximation for the surface energy anisotropy in Appendix B. The same assumption is also useful for the more precise numerical solution of the surface tension anisotropy presented in Sec. IV D.

Substitution of the ansatz (23) into Eq. (11) allows the free energy to be written as a function of ξ_1, ξ_2, ξ_3

$$F[a_1(\xi_1), a_2(\xi_2), a_3(\xi_3)] = F[f(\xi_1), f(\xi_2), f(\xi_3)], \tag{24}$$

$$= \tilde{F}(\xi_1, \xi_2, \xi_3). \tag{25}$$

The equations from which the optimal values of the correlation lengths are derived from are

$$\frac{d\tilde{F}}{d\xi_n} = \sum_{j=1}^{3} \int du \frac{\delta F}{\delta a_j(u)} \frac{da_j(u)}{d\xi_n}, \tag{26}$$

$$= -\frac{1}{\xi_n^2} \int duuf'(u/\xi_n) \frac{\delta F}{\delta a_n(u)} = 0, \tag{27}$$

where $\delta F/\delta a_n$ is obtained from Eq. (14) or one of its permutations. To make notation compact, we define

$$\langle h \rangle_n \equiv -\frac{1}{\xi_n^2} \int duuf'(u/\xi_n) h(u) \tag{28}$$

as a projection operation on $h(u)$, which will be applied to the individual terms of Eq. (14) following Eq. (26).

As will be numerically shown in Sec. V, we assume that the amplitudes a_n in Eq. (23) can be represented to reasonable accuracy as

$$a_n \approx f(u/\xi_n) \equiv c_s \tilde{f}(u/\xi_n), \tag{29}$$

$$\tilde{f}(x) \equiv \frac{1}{2}(\tanh(x) + 1). \tag{30}$$

The magnitude of c_s, which is the value of the amplitude a_n in the bulk, is typically assumed less than unity for weakly first order transitions [22].

C. Balancing the free energy wells of the three-amplitude model

Since the free energy in Eq. (1) is a truncated theory, the wells of the potential (12) are not generally balanced at coexistence. To enforce coexistence in the truncated multiamplitude theory, we consider a modification to the potential (12) of the following form:

$$V(a_1, a_2, a_3) \equiv \sum_n \alpha (a_n)^2 - \alpha_3 (a_1 a_2 a_3) + \alpha_4 \left\{ \frac{3}{2} \sum_n (a_n)^4 + 6[(a_1 a_2)^2 + (a_1 a_3)^2 + (a_2 a_3)^2] \right\}, \tag{31}$$

where

$$\alpha \equiv 3 - 2\hat{c}(q_0). \tag{32}$$

The phases Θ_n of the complex amplitudes have been set to zero. Two new parameters α_3 and α_4 can be determined from the extremal conditions

$$V(c_s, c_s, c_s) = V(c_l, c_l, c_l) = 0, \tag{33}$$

$$[dV(a_1, a_2, a_3)/da_n]|_{a_1 = a_2 = a_3 = c_s} = 0, \tag{34}$$

where c_s and c_l denote the dimensionless bulk amplitude values in the liquid and solid, respectively. The second equality in Eq. (33) is simply a consequence of the fact that $c_l = 0$. From these conditions, α_3 and α_4 can be fixed in two different ways that shall be indexed by "1" (for Shih *et al.* [30]) and "2" (for Wu *et al.* [22]). In the case (1) of Wu *et al.* [22], c_s is taken from molecular dynamics simulation and Eqs. (33) and (34) can be considered as two equations for two unknowns α_3 and α_4. In the case (2) of Shih *et al.* [30], the latent heat Δ_l is given in terms of α and α_4 as

$$\Delta_l = \frac{T_m}{2H'(T_m)} \left| \frac{\alpha}{\alpha_4} \right|, \tag{35}$$

where T_m is the melting temperature and $H'(T_m)$, is in the notation of Ref. [30], the temperature derivative of $12/S(k,T)$, where S is the structure factor. Equation (35) can be solved for α_4 in terms of Δ_l, leaving c_s and α_3 to be solved from Eqs. (33) and (34).

When expressed in terms of the bulk amplitude c_s, both ways of determining α_3 and α_4 will give rise to the same form of the evolution equations of the amplitude a_1:

$$\frac{m_1}{\alpha} \ddot{a}_1 = 2a_1 - \frac{6}{c_s} a_2 a_3 + \frac{12}{15 c_s^2} [a_1^3 + 2a_2(a_2^2 + a_3^2)] \tag{36}$$

(and similarly for amplitudes a_2 and a_3), where the bulk amplitude $c_s = c_{s1}$ or $c_s = c_{s2}$, with

$$c_{s1} \equiv [2\alpha/(15\alpha_4)]^{1/2}, \tag{37}$$

$$c_{s2} \equiv c_s \text{ from the MD simulation.} \tag{38}$$

The acronym MD stands for molecular dynamics. From Eq. (37) it follows that the magnitude of the c_s can become small if the latent heat of the substance is small.

It should be noted that by rescaling the amplitudes $a_n \to c_s a_n$ in Eq. (36) shows that c_s scales out of the Euler-

Lagrange equations. For higher order polynomial theories c_s cannot be scaled out. Moreover it is clear from Eq. (36) that α (or, M_2/α) can also be scaled out of the amplitude equations. This yields a prediction of the anisotropy that depends only on the form of the crystal structure selected by the model and not its specific materials parameters. This conclusion is consistent with the finding of Wu and Karma [29] and is also a consequence of a weakly fourth order nonlinear amplitude theory.

D. Nonlinear algebraic derivation of correlation lengths

This subsection derives a form of the correlation lengths from the full nonlinear amplitude model. These will be used in the next section to compute the surface energy and its anisotropy using Eqs. (23) and (18).

Applying the projection operator in Eq. (28) on the amplitude equation (14) yields

$$\frac{m_1}{\alpha}\langle \ddot{a}_1\rangle_1 = 2\langle a_1\rangle_1 - \frac{6}{c_s}\langle a_2 a_3\rangle_1 + \frac{12}{15c_s^2}(\langle a_1^3\rangle_1 + 2\langle a_1 a_2^2\rangle_1 + 2\langle a_1 a_3^2\rangle_1) \tag{39}$$

(and similarly for a_2 and a_3). Proceeding further we invoke Eq. (29) along with Eq. (30), which is shown to hold to reasonable accuracy in Sec. V. Using the specific form in Eq. (30) is done merely to arrive at an approximation of the anisotropy and its elucidate its angular form. Using different numerically determined $f_n(x)$'s for each amplitude will increase the accuracy of our results. The main physics and procedures outlined using the simple choice in Eq. (30) will, however, remain essentially unchanged. In terms of the correlation lengths, Eq. (39) thus becomes

$$\frac{\tilde{m}_1}{\alpha}\frac{1}{\xi_1^2} = B - 6W_1\left(\frac{\xi_1}{\xi_2},\frac{\xi_1}{\xi_3}\right) + \frac{24}{15}\left[W_2\left(\frac{\xi_1}{\xi_2}\right) + W_2\left(\frac{\xi_1}{\xi_3}\right)\right], \tag{40}$$

where

$$\tilde{m}_1 \equiv m_1 \int duu\tilde{f}'(u)\tilde{f}''(u), \tag{41}$$

$$B \equiv 2\int duu\tilde{f}'(u)\tilde{f}(u) + \frac{12}{15}\int duu\tilde{f}'(u)[\tilde{f}(u)]^3, \tag{42}$$

$$W_1(x,y) \equiv \int duu\tilde{f}'(u)\tilde{f}(ux)\tilde{f}(uy), \tag{43}$$

$$W_2(x) \equiv \int duu\tilde{f}'(u)\tilde{f}(u)[\tilde{f}(ux)]^2, \tag{44}$$

$$x \equiv \xi_1/\xi_2, \quad y \equiv \xi_1/\xi_3, \tag{45}$$

with m_1 given by Eq. (15), $\tilde{f}$ by Eq. (30), and α by Eq. (32).

By cyclically reshuffling the variables, three nonlinear equations for all correlation lengths are given as

$$\frac{\tilde{m}_1}{\alpha}\frac{1}{\xi_1^2} = B - 6W_1\left(\frac{\xi_1}{\xi_2},\frac{\xi_1}{\xi_3}\right) + \frac{24}{15}\left[W_2\left(\frac{\xi_1}{\xi_2}\right) + W_2\left(\frac{\xi_1}{\xi_3}\right)\right], \tag{46}$$

$$\frac{\tilde{m}_2}{\alpha}\frac{1}{\xi_2^2} = B - 6W_1\left(\frac{\xi_2}{\xi_1},\frac{\xi_2}{\xi_3}\right) + \frac{24}{15}\left[W_2\left(\frac{\xi_2}{\xi_1}\right) + W_2\left(\frac{\xi_2}{\xi_3}\right)\right], \tag{47}$$

$$\frac{\tilde{m}_3}{\alpha}\frac{1}{\xi_3^2} = B - 6W_1\left(\frac{\xi_3}{\xi_1},\frac{\xi_3}{\xi_2}\right) + \frac{24}{15}\left[W_2\left(\frac{\xi_3}{\xi_1}\right) + W_2\left(\frac{\xi_3}{\xi_2}\right)\right]. \tag{48}$$

Rescaling the ξ_n in Eqs. (46)–(48) according to

$$\tilde{\xi}_n \equiv h(T)\xi_n, \quad h(T) \equiv -2\frac{M_2(T,q_0)}{\alpha(T)}\int du\tilde{f}'(u)\tilde{f}''(u) \tag{49}$$

makes both sides of Eqs. (46)–(48) material independent. As discussed above, this is a consequence of the fourth order expansion of the amplitude equations and leads to a material-independent anisotropy. The isotropic part of the surface energy depends on the correlation function M_2 (which depends on T).

Equations (46)–(48) can be cast into a material-independent form by using Eq. (45). Dividing Eq. (46) by Eq. (47) and Eq. (46) by Eq. (48) gives

$$\frac{(\mathbf{K}_1\cdot\mathbf{n})^2}{(\mathbf{K}_2\cdot\mathbf{n})^2} = x^2\frac{B - 6W_1(x,y) + \frac{24}{15}[W_1(x) + W_1(y)]}{B - 6W_1\left(\frac{1}{x},\frac{y}{x}\right) + \frac{24}{15}\left[W_1\left(\frac{1}{x}\right) + W_1\left(\frac{y}{x}\right)\right]}, \tag{50}$$

$$\frac{(\mathbf{K}_1\cdot\mathbf{n})^2}{(\mathbf{K}_3\cdot\mathbf{n})^2} = y^2\frac{B - 6W_1(x,y) + \frac{24}{15}[W_1(x) + W_1(y)]}{B - 6W_1\left(\frac{1}{y},\frac{x}{y}\right) + \frac{24}{15}\left[W_1\left(\frac{1}{y}\right) + W_1\left(\frac{x}{y}\right)\right]}. \tag{51}$$

Once the solutions $x=x^*$ and $y=y^*$ are found from Eqs. (50) and (51), the correlation length ξ_1 is found from Eq. (46)

$$\xi_1 = \left(\frac{\tilde{m}_1/\alpha}{B - 6W_1(x^*,y^*) + \frac{24}{15}[W_1(x^*) + W_1(y^*)]}\right)^{1/2} \tag{52}$$

and ξ_2 and ξ_3 are given by Eq. (45).

Equations (50) and (51) are universally true for any 2D hexagonal crystal represented by a fourth order amplitudes model, and for which the dimensionless average density jump $\Delta\rho=0$. The prefactors appearing in Eqs. (50) and (51) have different numerical values for the case $\Delta\rho\neq 0$, as discussed in Appendix C.

In the next section the algebraic equations will be numerically solved for the correlation lengths ξ_i. These lengths will

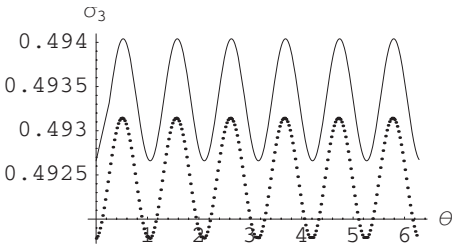

FIG. 1. Anisotropic surface tension as a function of θ from the algebraic method. The cosine fit (solid line) has been shifted in the y direction. Adjacent dots in the plot are spaced 0.025 radians apart.

then be used to approximate the magnitude and anisotropy of the surface tension of a two-dimensional crystal. Appendix C shows a simpler (and different) example where the correlation lengths are calculated analytically and used to calculate a crude approximation of the form of the anisotropy.

V. NUMERICAL DETERMINATION OF SURFACE ENERGY

This section compares the results of the algebraic method presented in the previous section to the numerical solution of the full Euler-Lagrange equations for the real amplitudes (14) with suitable boundary conditions, which are then substituted back into the free energy (11) to obtain the surface energy and its anisotropy. In the latter case no simplifying assumptions are used contrary to the former method, which utilizes the scaling forms (29) and (30).

The total surface energy $\sigma_3(\theta)$ computed using Eqs. (23) and (18), and the ξ_n^* from Sec. IV D is plotted in Fig. 1. The continuous line indicates the best fit $\sigma_3^{\text{fit}}(\theta)=0.49245+0.00069\cos(6\theta+\pi)$, where the total number of data points is 250 taken at intervals $\Delta\theta=0.025$ rad ($\approx 2\pi/250$). When expressed in the form of Eq. (19), the anisotropy factor ϵ becomes $0.00069/0.49245\approx 0.14\%$.

Figure 2 compares the total surface energy from the algebraic method (lower curve) and from the direct solution of the Euler-Lagrange equations (14) (upper curve). In the direct solution of the Euler-Lagrange equations a value of $\alpha=1.0$ was used, while $c_s=1.0$ was used for the far-field amplitude and $M_2=1.0$. The algebraic method gives an anistropy $\sim 0.14\%$ whereas the full Euler-Lagrange solution yields $\sim 0.20\%$. Hence, the value of the anistropy $\sim 0.1-0.2$ % is consistent with both methods. As for the isotropic parts, the difference between the two methods is of the order $\sim 0.1\%$. Solving the full Euler-Lagrange equation with other values of α yielded the same result. As discussed above, this is a consequence of Eqs. (18) and (36), which allow the spatial argument of a_n to be rescaled so that all materials and temperature dependences are transferred into the isotropic part of surface tension but not the anisotropy ϵ.

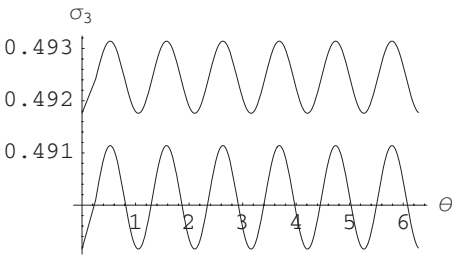

FIG. 2. Comparison of the anisotropies obtained from the algebraic (upper curve) method and the direct solution of the Euler-Lagrange equations (lower curve).

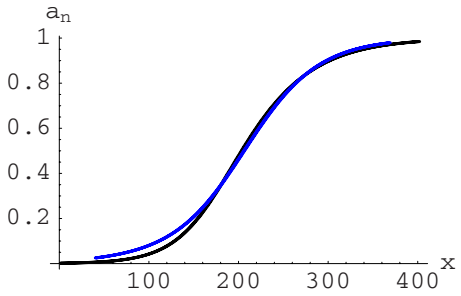

FIG. 3. (Color online) Amplitude profiles are not perfectly self-affine. The blue curve $a_2(x)$ and the black curve $a_1(kx)$, where $k=0.82$ has been chosen to maxize the overlap ($\theta=0.025$). The curves are entirely overlapping for $x\geqslant 170$ (in the units of the lattice constant a) whereas for the smaller values a_2 rises slightly above a_1.

The difference in the two methods originates from two factors. First, there is a small dependence on $n=1,2,3$ (the amplitude index) in the Euler-Lagrange solutions for the amplitudes as shown in Fig. 3, which shows the best scaling collapse for a_1 and a_2 (a_2 and a_3 are practically overlapping). As can be seen from Fig. 3 there is no perfect common scaling behavior for distances less than ~ 150 in the units of lattice spacing Δx. The second reason for the lack of complete overlap in Fig. 2 is due to the slight deviation of the a_n from the tanh-ansatz (30), which was utilized in Eq. (39). The deviations, depicted in Figs. 4 and 5, while small, are large enough to cause the algebraic and Euler-Lagrange methods to deviate by $\sim 0.1\%$ in the total surface tension.

Figure 6 illustrates the stifness $\sigma_3(\theta)+\sigma_3''(\theta)$, where $\tan\theta=\partial_y a/\partial_x a$. Due to the second derivative σ_3'' even a small anisotropy can give rise to strongly nonconvex shapes in contrast to the Wulff plot, which is practically a circle for anisotropies less than 1%.

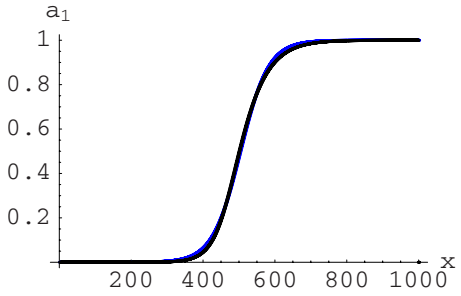

FIG. 4. (Color online) tanh-like profile fits to amplitudes over the entire range of x as in Fig. 3 (with x in the same units). On the scale of the figure the tanh fit (blue curve) of the form $a(x)=(1/2)\tanh[(x-x_0)/\xi]$ with fitting parameters ξ and x_0 is indistinguishable from the simulated result a_1 (black line). See enlargements in Fig. 5 for deviations.

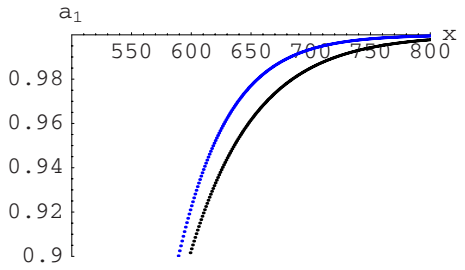

FIG. 5. (Color online) Enlargement of the top-right shoulder region in Fig. 4 reveals a deviation of the simulated profile (lower black curve) from the fitted tanh shape (upper blue curve). The x axis is in the same units as Fig. 3.

Dimensionality has an effect on the surface energy anisotropy. Various definitions and calculations of anisotropy have been reported in the literature with values ranging from 0.4–1 % in 3D [22,33]. In 3D there are more directions (see Fig. 7) in the reciprocal lattice vector space and consequently there are larger differences in the free energy barriers between these directions. This is illustrated in Fig. 8, obtained using a truncated analytic method analogous to Eq. (B8) for a corresponding 3D bcc lattice. For a specific azimuthal angle $\varphi=0.8$ the anisotropy of the bcc crystal is $\sim 11.5\%$, roughly double the 6.7% quoted in Eq. (B9). The results of the truncated series are not quantitatively correct as they will be renormalized by nonlinearities in 2D and 3D as seen from the numerical results of Fig. 2. Nevertheless, these approximate anisotropies indicate that the 3D anisotropy can be significantly higher than its 2D counterpart.

The larger differences in the free energy landscape in 3D compared to 2D are also consistent with the fact that in general surfaces are less rigid in 2D than in 3D. Ising-type models with short-range interactions exhibit a roughening transition, which takes place at $T=0$ in 2D and at $T=T_r>0$ in 3D destroying the faceted structure when the crystal surface width diverges as a function of the system size L [34]. In 2D, faceted structures can therefore only exist as metastable states, in the mean-field sense with zero noise.

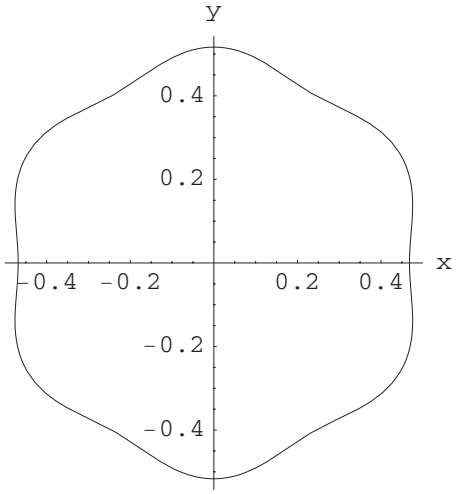

FIG. 6. Stifness plot as a function of the angle θ for the three amplitude model.

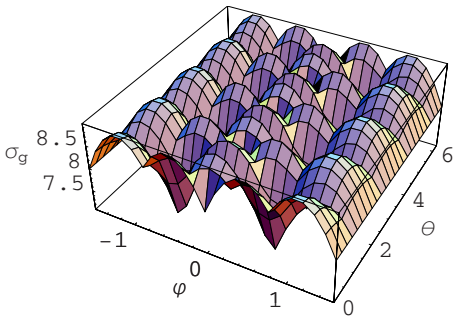

FIG. 7. (Color online) Surface tension $\sigma_g(\theta,\varphi)$ using the 3D analog of Eq. (B8) for bcc crystal.

We note that surface anisotropies of short-range lattice models [35] and their continuum generalizations are expected to be temperature dependent. In the frame work of the model presented in this work (suitable for weakly first-order transitions [29]), however, the temperature dependence of anisotropy is expected to be less than $\sim 0.1\%$, the difference in the methodologies depicted in Fig. 2. This is because there is no temperature or materials dependence in the anisotropy determined by the method of Sec. IV D.

VI. EFFECTIVE PROCEDURE FOR COARSE GRAINING

It is instructive to consider how to construct the potential part V_1 of a single-order parameter theory from our three parameter theory. To do so, we use the following simple replacement rule:

$$V_1(g) \equiv V(g,g,g), \tag{53}$$

where V is the potential of the three amplitude theory Eq. (31) and g satisfies the same scaling form as Eq. (23) for f but has a different effective correlation length. There are infinitely many potentials which could be chosen as far as only the surface tension of the single order parameter model is considered. This is due to the relations (16) and (18). However, fixing V_1 will affect f_n and in the present construction all f_n are assumed (to a good approximation) to be independent of the index n. Only then does the gradient part of the free energy reduce to a form whose prefactor can be easily

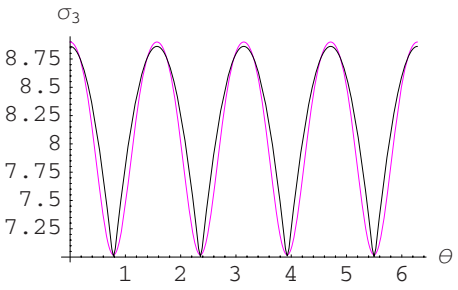

FIG. 8. (Color online) $\varphi=0.8$ plane cut of Fig. 7 showing $\sigma_g(\theta,0.8)$ (black curve). The azimuthal angle $\varphi=0.8$ yields an effective four-fold anisotropy locally. The purple curve is a three-parameter (d_1,d_2,d_3) fit to $d_0+d_1\cos(4\theta)+d_2\cos^2(4\theta)$. The two curves are almost entirely overlapping on the scale of the plot. The angle Θ takes values in the interval $[0,2\pi]$ rad.

fixed. The direction-dependent surface energy of the three amplitude theory is given by

$$\sigma_3(\theta) = \int du \left\{ \frac{1}{2}\sum_n m_n \left[\frac{d}{du} f^*\left(\frac{u}{\xi_n}\right)\right]^2 + V\left[f^*\left(\frac{u}{\xi_1}\right), f^*\left(\frac{u}{\xi_2}\right), f^*\left(\frac{u}{\xi_3}\right)\right]\right\} \tag{54}$$

$$= \int du \sum_n m_n \left[\frac{d}{du} f^*\left(\frac{u}{\xi_n}\right)\right]^2. \tag{55}$$

This surface energy can now be obtained from the procedure of Sec. V, namely, solving numerically for ξ_n^* and obtaining an expansion of the form of Eq. (19) (see also Appendix B to justify this expansion). The magnitude of the higher order anisotropies in the cosine series are expected to diminish fast with increasing power of the cosine.

The gradient energy coefficient $w_1^2(\theta)$ can be fixed in of an effective single amplitude theory in such a way that surface energy will be given by $\sigma_3(\theta)$. Comparing the single amplitude free energy

$$F_S[g] \equiv \int d\mathbf{r} \left\{ \frac{1}{2} w_1^2(\theta) |\nabla g(\mathbf{r})|^2 + V_1[g(\mathbf{r})]\right\} \tag{56}$$

to Eq. (54), we obtain

$$w_1(\theta) = \frac{\sigma_3(\theta)}{(c_s/2)^2 \tilde{\alpha}^{1/2} \int du [\tilde{f}(u)]^2}, \tag{57}$$

where Eqs. (B13), (B14), and (B16) have been used, along with the assumptions that $\xi \equiv w/\sqrt{\tilde{\alpha}}$ and that the solution of the Euler-Lagrange equation of the single-order parameter theory $g^*(u) \approx (c_s/2)[\tanh(u/\xi)+1]$, where, in general, $\xi \neq \xi_1, \xi_2, \xi_3$. The determination of $\tilde{\alpha}$ has been discussed in Appendix B 2. To work with a general g^*, without making the assumptions above, solving the self-consistent equation for w^2 becomes much harder.

Since the order parameter of a theory is not unique, one could, for example, use the mean amplitude or the geometric mean of a_1, a_2, and a_3 as the effective single-order parameter. These have simple mathematical expressions, and their interpretation is easy (mathematically and physically). However, the technical computation of F_S becomes extremely hard in these cases, at least when derived by removing degrees of freedom from the partition function defining F_S.

VII. CONCLUSIONS

Coarse graining of a simple classical density functional theory (DFT) for freezing of a pure material was presented. The form of a three-amplitude representation of the original free energy was derived. The surface energy and the orientational dependence of its anisotropy was calculated analytically and numerically for a 2D hexagonal crystal at coexistence with a liquid. It was also demonstrated numerically and analytically that the general form of the anisotropy for the simple classical density functional theory used here can be expressed as power series in $\cos(6\theta)$, for hexagonal 2D materials. The procedures presented in this work can also be generalized to 3D and to higher order density wave expansions.

The techniques developed in this work constitute a step towards deriving thermodynamically consistent phase-field-type models from fundamental microscopic theories, which self-consistently incorporates atomic-scale properties. This approach can have several important applications in microstructure modeling. These include the prediction of surface energy and its anisotropy, and more realistic phase-field free energies than those typically generated by phenomenological phase-field approaches.

In general, fourth-order truncation of the bulk potential in the free energy can distort the phase diagram significantly despite the fact that the latent heat can be fitted correctly with a fourth-order expansion. Future studies will address a more systematic technique for including higher order local terms in the potential part reference free energy as well as the parametrization of nonlocal correlations in F.

ACKNOWLEDGMENTS

N.P. acknowledges the National Science and Engineering Research Council of Canada (NSERC) and the Canadian Space Agency (CSA) for funding.

APPENDIX A: LOCAL VOLUME AVERAGING

In this work, local volume averaging, or box averaging, uses the following convolution kernel together with a noninvertible limiting procedure;

$$\langle f(x)\rangle_L \equiv \frac{1}{\sqrt{\pi}L} \int_{-\infty}^{\infty} dx' e^{-(x-x')^2/L^2} f(x'), \tag{A1}$$

$$\equiv \int_{-\infty}^{\infty} dx' \chi_L(x-x') f(x'). \tag{A2}$$

Consider as an example coarse graining a rapidly oscillating field $\rho(x)$, expressed as a density wave expansion in 1D with x-dependent amplitudes as introduced in Eq. (5). Assume further that these amplitudes contain Fourier modes k satisfying $|Lk| \ll 1$. This gives

$$\langle \rho(x)\rangle_L = \bar{\rho}_0 + \sum_{n=1}^{3} \langle a^n(x) e^{\imath K^n x}\rangle_L, \tag{A3}$$

$$\approx \bar{\rho}_0 + \sum_{n=1}^{3} \langle a^n(x)\rangle_L \langle e^{\imath K^n x}\rangle_L, \tag{A4}$$

$$\approx \bar{\rho}_0 + \sum_{n=1}^{3} a^n(x) e^{-(LK^n)^2/4}, \tag{A5}$$

where $\bar{\rho}_0$ is a constant equal to 1 in the unit convention used above. In this case the latter sum vanishes in comparison with the constant term. Physically this implies that $a^n(x)$ is

very slowly varying over the scale on which the phase factor oscillates, allowing it to decouple from the average of the phase factor. If a function such as $[\rho_0(x)]^2$ is averaged, some terms emerge that contain wave vector combinations that sum up to zero. These terms correspond to slowly varying terms that do not vanish.

In general, spatial coarse graining can be carried out by applying Eq. (A1) to a functional of the free energy density $f(x) \equiv f[\rho(x)]$ as follows:

$$F[\rho] = \int dx' f(x') = \int dx' \left(\int dx \chi_L(x - x') \right) f(x') = \int dx \int dx' \chi_L(x - x') f(x') = \int dx \langle f(x) \rangle_L. \quad \text{(A6)}$$

Assume that $f(x)$ can be decomposed into a series of wave modes of the form $e^{\imath kx}$. For $L \gg 1/k_c$ where k_c represents some cutoff frequency, the volume average of $f(x)$ then satisfies

$$\lim_{k_c L \gg 1} \int dx \langle f(x) \rangle_L = \int dx \lim_{k_c L \gg 1} \langle f(x) \rangle_L. \quad \text{(A7)}$$

The notation $\lim_{k_c L \gg 1}$ implies that for all wave vectors $k \geqslant k_c$ $[=O(|\mathbf{K}^n|)$ in this work] in the Fourier decomposition of f, the product $k_c L$ can effectively be taken to infinity.

Equation (A7) introduces the irreversibility into the coarse-graining operation by switching the order of the limit and the integration. Hence all modes of the function $f(x)$ greater than $k \sim |k_c|$ will become exponentially suppressed and vanish from the description (will be set to zero) as L becomes much larger than $1/k_c$.

In the irreversible limit where $|\mathbf{K}^n L|$ is kept finite, the exponentially damped terms that arise from the volume averaging remain in the free energy. This strictly violates the exact translational invariance of the free energy under uniform space translations. For a density decomposition with only a finite number of spatially dependent amplitudes [Eq. (5)] these corrections are expected to be small and can formally be eliminated by taking the irreversible box-averaging limit $|\mathbf{K}^n L| \to \infty$.

In this work the box-averaging procedure defined by Eqs. (A6) and (A7) (extendable to two or three spatial dimensions) is be performed on terms of the form $\sim f[a(\mathbf{r})] e^{-\imath \Delta \vec{K} \cdot \mathbf{r}}$, where $\Delta \vec{K}$ is a sum or difference of the reciprocal lattice vectors $\mathbf{K}^n(\mathbf{r})$ (e.g., the free energy components F_A, F_B, and F_C). Since all reciprocal lattice vectors are comparable to q_0, the net effect of volume averaging technique is that only terms that contain sums of wave vectors that sum to zero contribute a finite value to the volume average. Others essentially cause the volume average to vanish.

APPENDIX B: ORIGIN OF THE ANGULAR FORM ANISOTROPY

1. Three amplitude model

To obtain crude estimates of the isotropic part of the surface energy, as well as the functional dependence of its anisotropy on the angle θ, it is instructive to consider only the first term on the right-hand side of Eq. (14). In dimensional units (used through these appendixes), this leads to

$$m_n \langle \ddot{a}_n \rangle_n \approx 2 \left(\frac{3}{\bar{\rho}_0} - 2\hat{c}(q_0) \right) \langle a_n \rangle_n \quad \text{(B1)}$$

when Eq. (14) is substituted into Eq. (26). This assumption will be dropped in Sec. IV D. It is emphasized that Eq. (B1) can only be considered an expansion in small c_s (weakly first-order transition) if c_s is independent of $\bar{\rho}_0$, which is not generally true (see Eq. (37), which reads $c_{s1} = [2\bar{\rho}_0^3 \alpha/(15\alpha_4)]^{1/2}$ in the units where $\bar{\rho}_0$ appears explicitly). Using the projection operation in Eq. (28), Eq. (B1) can be cast as

$$\frac{m_n}{(\xi_n^*)^2} \int duuf'(u) f''(u) \approx 2\alpha \int duuf'(u) f(u) \quad \text{(B2)}$$

for $n = \{1, 2, 3\}$. Equation (B2) gives the leading order correlation lengths as

$$\xi_n^* \approx \gamma \sqrt{m_n}, \quad \text{(B3)}$$

where

$$\gamma \equiv \sqrt{\frac{\int duuf'(u) f''(u)}{2\alpha \int duuf'(u) f(u)}}. \quad \text{(B4)}$$

Substituting Eq. (23) into Eq. (18), with $\xi_n = \xi_n^*$, gives the surface energy σ of the three-order parameter theory of Sec. III B as

$$\sigma_3(\theta) = \int du \sum_n m_n \dot{a}_n^2 = \sigma_0 \sum_n |\mathbf{K}^n \cdot \mathbf{n}|, \quad \text{(B5)}$$

where

$$\sigma_0 \equiv \frac{\sqrt{-2M_2}}{\gamma} \int du [f'(u)]^2. \quad \text{(B6)}$$

The geometric part of Eq. (B5) gives an isotropic and anisotropic contribution to the surface energy σ, to the order or approximation considered in this subsection. Specifically,

$$\sum_n |\mathbf{K}^n \cdot \mathbf{n}| = |\sin\theta| + \left| -\frac{\sqrt{3}}{2} \cos\theta - \frac{1}{2} \sin\theta \right| + \left| \frac{\sqrt{3}}{2} \cos\theta - \frac{1}{2} \sin\theta \right|. \quad \text{(B7)}$$

Using the relation between Chebychev polynomials of sixth order and $\cos\theta$, one can express Eq. (B7) as an infinite power series in the variable $\cos(6\theta)$. Analytically this requires a complicated inversion process, which is approxi-

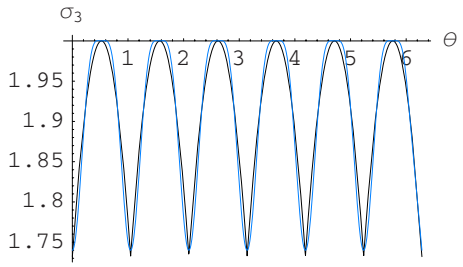

FIG. 9. (Color online) 2D surface tension vs θ (in radians) using the truncated algebraic solution (B7) (black line). The blue line is the fit to Eq. (B8). The two curves are almost entirely overlapping on the scale of the plot.

mated here numerically to first order in $\cos(6\theta)$ according to

$$\sigma_g(\theta) \equiv \sum_n |\mathbf{K}^n \cdot \mathbf{n}| \approx 1.94 - 0.13\cos(6\theta) - 0.07\cos^2(6\theta). \tag{B8}$$

This function is given by the continuous line in Fig. 9. The isotropic contribution approaches $\sigma_g(\pi/12) \approx 1.932$, and the strength of the anisotropy, as evaluated from Eq. (B8), is

$$\epsilon = \frac{0.13}{1.94} \approx 0.067. \tag{B9}$$

To leading order, the anisotropy parameter ϵ is only dependent on the geometry. Its renormalization due to the effect of the nonlinear contributions from Eq. (14) will studied in Sec. IV D.

To extract the complete isotropic part of the approximate three amplitude theory σ_3^{iso}, we utilize the cosine-series representation of Eq. (B8), whose oscillating contribution vanishes when evaluated at $\theta = \pi/12$. Specifically, combining Eqs. (B5) and (B7) gives

$$\sigma_3^{\text{iso}} = \sigma_0 \sigma_g(\pi/12), \tag{B10}$$

$$= P_3 \sqrt{-2M_2}\sqrt{2\alpha} \int du[f'(u)]^2, \tag{B11}$$

where

$$P_3 \equiv \left[\sqrt{\frac{\int duuf'(u)f(u)}{\int duuf'(u)f''(u)}} \sigma_g(\pi/12) \right]. \tag{B12}$$

2. Single amplitude derivation of isotropic surface tension

As a consistency check, we consider the isotropic surface energy from a theory where all the three amplitudes are the same: $a_n = a$ in Eq. (11). In the (s,u) curvlinear (s,u)-surface coordinate representation, where u is the normal to the interface and s is the coordinate along the phase boundary curve,

$$\frac{F}{L_y} = \int du \left\{ \frac{1}{2} w^2 \dot{a}^2 + V_1(a) \right\}, \tag{B13}$$

where $w^2 \equiv \Sigma_{n=1}^3 m_n$ and

$$V_1 \equiv 3\alpha a^2 - \frac{1}{\bar{\rho}_0^2} a^3 + \frac{45}{2\bar{\rho}_0^3} a^4. \tag{B14}$$

The wells of V_1 can be balanced for two-phase coexistence by tuning the coefficients of the third and fourth order terms in V (see Sec. IV C). Alternatively, one can add a constant chemical potential term μ_0 to the free energy (B13) to determine the surface tension. Specifically, a shift $a \to a + \text{const}$ can be performed together with rescaling of a in such a way that the odd terms vanish from V_1 once μ_0 is chosen correctly. Equation (B13) then becomes

$$\frac{F}{L_y} = \int du \left\{ \frac{1}{2}(wc_s)^2 (\partial_u \tilde{f})^2 + \frac{45c_s^4}{2\bar{\rho}_0^3} (\tilde{f}^2 - 1)^2 \right\}. \tag{B15}$$

This is of the standard ϕ^4 form and, consequently, the extremal solution $\tilde{f} = \tanh(u/\xi)$, with $\xi \equiv \frac{w}{\sqrt{\tilde{\alpha}}}$ and

$$\tilde{\alpha} \equiv 3\alpha - \frac{3c_s}{\bar{\rho}_0^2} + \frac{135c_s^2}{2\bar{\rho}_0^3}. \tag{B16}$$

The denominator $\tilde{\alpha}$ collects contribution from all terms in V_1 due to the shift which was performed to eliminate the third order term in V_1.

Approximating $\tilde{\alpha} \approx 3\alpha$ in Eq. (B16) makes it possible to compare terms of the same order as that in the three amplitude theory of Sec. B1. Specifically, the effective single amplitude isotropic surface energy becomes

$$\sigma_1^{\text{iso}} \equiv \frac{F[a^*]}{L_y} = \frac{w^2}{\xi} \int du[f'(u)]^2 \tag{B17}$$

$$= w\sqrt{\tilde{\alpha}} \int du[f'(u)]^2. \tag{B18}$$

(Note that the amplitude f is proportional to c_s). Since $w^2 = \Sigma_n m_n = (3/2)(-2M_2)$ which can be seen from Eqs. (15) and (6), we thus obtain

$$\sigma_1^{\text{iso}} = \sqrt{\frac{3}{2}}\sqrt{-2M_2}\sqrt{\tilde{\alpha}} \int du[f'(u)]^2, \tag{B19}$$

$$\approx \frac{3}{2}\sqrt{-2M_2}\sqrt{2\alpha} \int du[f'(u)]^2. \tag{B20}$$

Comparing this with the three amplitude result (B11) shows that the expressions are the same except for the factors 3/2 in Eq. (B20) and P_3 in Eq. (B12). Numerically, however, it turns out that $P_3 \approx 1.57$ and thus the isotropic surface tensions from the two different methods (Appendixes B 1 and B 2) agree within the accuracy of 4%, which is of the same order of magnitude as the anistropy 6.7%. However, we note that neither σ_1^{iso} nor σ_3^{iso} is exactly correct. To determine the isotropic as well as anistropic contributions more precisely, the numerical techniques presented in Sec. IV D are used.

APPENDIX C: SOLID-LIQUID DENSITY JUMP

A more complete density expansion than Eq. (5) can include higher order modes or a nonzero $\Delta\rho$ density jump be-

tween solid and liquid phases. The latter can be included as follows:

$$\rho(\mathbf{r}) = \bar{\rho}_0 + \Delta\rho(\mathbf{r}) + \sum_{n=1}^{3} A_n(\mathbf{r}) e^{i\mathbf{K}^n\cdot\mathbf{r}} + \text{c.c.} \qquad \text{(C1)}$$

In general, however, the density difference between the solid and its melt is very small, especially as compared to the density jump between the liquid and gas phases [36].

In the existing literature on the phase-field crystal models the effects of $\Delta\rho$ have not been explicitly considered in density expansions despite the fact that both the phase diagram and the simulations confirm that a nonzero $\Delta\rho$ exists. It is argued that one-mode density expansions are only valid close to the spinodal, where $\Delta\rho$ is very small. On the other hand, in freezing literature it has been argued that neglecting $\Delta\rho$ without considering simultaneously the compressiblity [which is controlled by $\hat{c}(0)$] in Ramakrishnan-Yussouff–type density functional theories [37] leads to a qualitatively and quantitatively inaccurate description. For almost incompressible melts one can set $\Delta\rho \to 0$ and $\hat{c}(0) \to -\infty$ by keeping the combination $\hat{c}(0)\Delta\rho$ finite [38].

At the level of the Euler-Lagrange equations $\Delta\rho$ represents a new independent field which is coupled with $a_n(\mathbf{k})$ and therefore can have an effect on the surface tension. An explicit expression for the surface tension in Ramakrishnan-Yussouff–type theory has been provided for a spatially slowly varying density jump in Ref. [38]. Despite the coupling in Euler-Lagrange equations, $\Delta\rho$ can behave in the dynamic sense "independently" of the modes a_n. Specifically, $\Delta\rho$ stays constant during the first structuring stage of crystallization, which largely involves enhancement of the amplitudes a_n, with $\Delta\rho$ changing only later [39].

In the case of the present theory, the effects of a nonzero $\Delta\rho$ can be included in the first-order approximation as follows. By substituting the density expansion (C1) into F box averaging and assuming small $\Delta\rho$ close to a spinodal, the order $(\Delta\rho)^2$ contribution to F can be worked out. Following the same argumentation as in Ref. [30], by extremizing F with respect to $\Delta\rho$ and back substituting the result into F, the coefficient of the fourth-order amplitude term becomes renormalized, $F \to F + \Delta F$, where

$$\Delta F \approx -\frac{h}{\bar{\rho}_0^3}\left(\sum_n a_n^2\right)^2 \qquad \text{(C2)}$$

with $h = 1/24$ in our three amplitude model. The estimate presented in Eq. (C2) represents the upper bound with the inclusion of $O(\Delta^2)$ terms. A gradient term $c''(0)|\nabla\Delta\rho|^2$ has been left out due to the smallness of $c''(0)$, and it is this assumption [38] that turns the Euler-Lagrange equation for $\Delta\rho$ into an algebraic equation approximately satisfying Eq. (C2). Consequently, the prefactors of the third- and fourth-order terms of the free energy $F + \Delta F$ will change as compared to those of F, resulting in the change of the values of α_3 and α_4. The effect of these changes turns out to be quantitatively very small on the anisotropy, for $h = 1/24$. There are values of h for which the difference becomes larger but not all of them are expected to be physically accessible.

These findings are consistent with the observation presented in Ref. [40], which shows that for phenomenologically adjusted free energies the contribution to the surface energy from a_n is about 10 to 100 times larger than the contribution from the density jump. Finally, it is pointed out that the form of the equations of motion is not affected whether one uses $F + \Delta F$ or F.

[1] R. Almgren, SIAM J. Appl. Math. **59**, 2086 (1999).
[2] A. Karma and W.-J. Rappel, Phys. Rev. E **53**, R3017 (1996).
[3] A. Karma, Phys. Rev. Lett. **87**, 115701 (2001).
[4] B. Echebarria, R. Folch, A. Karma, and M. Plapp, Phys. Rev. E **70**, 061604 (2004).
[5] N. Provatas, M. Greenwood, B. Athreya, N. Goldenfeld, and J. Dantzig, Int. J. Mod. Phys. B **19**, 4525 (2005).
[6] R. Folch and M. Plapp, Phys. Rev. E **72**, 011602 (2005).
[7] C. Tong, M. Greenwood, and N. Provatas, Phys. Rev. B **77**, 064112 (2008).
[8] N. Provatas, N. Goldenfeld, J. Dantzig, J. C. LaCombe, A. Lupulescu, M. B. Koss, M. E. Glicksman, and R. Almgren, Phys. Rev. Lett. **82**, 4496 (1999).
[9] M. Plapp and A. Karma, J. Comput. Phys. **165**, 592 (2000).
[10] M. Sabouri-Ghomi, N. Provatas, and M. Grant, Phys. Rev. Lett. **86**, 5084 (2001).
[11] J. Bragard, A. Karma, Y. H. Lee, and M. Plapp, Interface Sci. **10**, 121 (2002).
[12] M. Greenwood, M. Haataja, and N. Provatas, Phys. Rev. Lett. **93**, 246101 (2004).
[13] J. Hoyt, M. Asta, and A. Karma, Mater. Sci. Eng. R. **41**, 121 (2003).
[14] K. R. Elder, M. Katakowski, M. Haataja, and M. Grant, Phys. Rev. Lett. **88**, 245701 (2002).
[15] K. R. Elder and M. Grant, Phys. Rev. E **70**, 051605 (2004).
[16] J. Berry, K. Elder, and M. Grant, Phys. Rev. E **73**, 031609 (2006).
[17] P. Stefanovic, M. Haataja, and N. Provatas, Phys. Rev. Lett. **96**, 225504 (2006).
[18] K. R. Elder, N. Provatas, J. Berry, P. Stefanovic, and M. Grant, Phys. Rev. B **75**, 064107 (2007).
[19] N. Provatas, J. Dantzig, B. P. Athreya, P. Chen, P. Stefanovic, N. Goldenfeld, and K. Elder, JOM **59**, 83 (2007).
[20] C. V. Achim, M. Karttunen, K. R. Elder, E. Granato, T. Ala-Nissila, and S. C. Ying, Phys. Rev. E **74**, 021104 (2006).
[21] Y. M. Jin and A. Khachaturyan, J. Appl. Phys. **100**, 013519 (2006).
[22] K. A. Wu, A. Karma, J. J. Hoyt, and M. Asta, Phys. Rev. B **73**, 094101 (2006).
[23] S. Majaniemi and M. Grant, Phys. Rev. B **75**, 054301 (2007).
[24] S. Majaniemi, M. Nonomura, and M. Grant, Eur. Phys. J. B **66**, 329 (2008).
[25] N. Goldenfeld, B. P. Athreya, and J. A. Dantzig, Phys. Rev. E **72**, 020601(R) (2005).

[26] B. P. Athreya, N. Goldenfeld, J. A. Dantzig, M. Greenwood, and N. Provatas Phys. Rev. E **76**, 056706 (2007).
[27] L. V. Mikheev and A. A. Chernov, J. Cryst. Growth **112**, 591 (1991).
[28] G. Szamel, J. Stat. Phys. **87**, 1067 (1997).
[29] K. A. Wu and A. Karma, Phys. Rev. B **76**, 184107 (2007).
[30] W. H. Shih, Z. Q. Wang, X. C. Zeng, and D. Stroud, Phys. Rev. A **35**, 2611 (1987).
[31] B. Grossmann, K. R. Elder, M. Grant, and J. M. Kosterlitz, Phys. Rev. Lett. **71**, 3323 (1993).
[32] N. Provatas, T. Ala-Nissila, M. Grant, K. Elder, and L. Piche, J. Stat. Phys. **81**, 737 (1995).
[33] D. Y. Sun, M. Asta, J. J. Hoyt, M. I. Mendelev, and D. J. Srolovitz, Phys. Rev. B **69**, 020102(R) (2004).
[34] K. K. Mon, S. Wansleben, D. P. Landau, and K. Binder, Phys. Rev. Lett. **60**, 708 (1988).
[35] C. Rottman and M. Wortis, Phys. Rev. B **24**, 6274 (1981).
[36] A. D. J. Haymet and D. W. Oxtoby, J. Chem. Phys. **74**, 2559 (1981).
[37] T. V. Ramakrishnan and M. Yussouff, Phys. Rev. B **19**, 2775 (1979).
[38] D. W. Oxtoby and A. D. J. Haymet, J. Chem. Phys. **76**, 6262 (1982).
[39] D. W. Oxtoby, Acc. Chem. Res. **31**, 91 (1998).
[40] D. W. Oxtoby and P. R. Harrowell, J. Chem. Phys. **96**, 3834 (1992).